Max-Planck-Institut
für Mathematik
in den Naturwissenschaften
Leipzig

Multiscale Modeling of Materials - the Role of Analysis

by

Sergio Conti, Antonio DeSimone, Georg Dolzmann, Stefan Müller, and Felix Otto

Preprint no.: 1 2002

Multiscale Modeling of Materials – the Role of Analysis

S. Conti,[1] **A. DeSimone,**[1] **G. Dolzmann,**[2]
S. Müller,[1] **F. Otto**[3]
[1] Max–Planck–Institute for Mathematics in the Sciences,
Inselstraße 22–26, 04103 Leipzig
[2] Department of Mathematics, University of Maryland,
College Park MD 20742, USA
[3] Institut für Angewandte Mathematik,
Wegelerstraße 10, 53115 Bonn

January 1, 2002

Abstract: We present two case studies how analysis can be used to derive a hierarchy of models to capture multiscale behavior of materials. The determination, via Γ–convergence, of the thin film limit of micromagnetism delivers a reduced two–dimensional model for soft ferromagnetic films which justifies previously known theories for small fields and extends them to the regime of field penetration. The analytic evaluation of the quasiconvex envelope of the microscopic energy density of nematic elastomers allows efficient numerical computations with finite elements and shows the existence of a new "smectic" phase. In both cases, the numerical solution of the coarse–grained model is complemented by a reconstruction of the microscopic pattern associated with the reduced field.

1 Introduction

The behavior of natural and artificial materials is often determined by complex internal patterns spanning several different length scales, from the atomic to the macroscopic one. Proper understanding of the microstructure, and of ways to influence it, has often led to progress in the development of new materials. Classical approaches are based on intuition and experimental evidence, but recently increasing importance has been given to a complementary approach, based on modeling and simulation. Progress in atomistic molecular dynamics and *ab initio* quantum–mechanical simulations deliver precise

information on the behavior of individual molecules, or of systems where a relatively small group of atoms is present. However, in many cases the relevant structures arise through collective effects, which involve huge numbers of atoms. A full quantum–mechanical, or even atomistic, computation of such systems is clearly unfeasible, and also not desirable from the point of view of qualitative understanding. It is therefore important to develop and apply methods which allow one to systematically transform the information available on the small scales into an effective model which describes the large scales alone.

In the last decades powerful mathematical tools have been developed to pass from models on microscopic or mesoscopic scales to macroscopic ones, within the general framework of weak–convergence methods. The ideas of Γ–convergence [19, 20, 18], relaxation [15], homogenization [49, 39, 10], quasiconvexification [46, 16, 47], Young–measures and compensated compactness [63, 55], H–measures [56, 33] and their variants provide general techniques which allow one, in principle, to derive rigorously large–scale effective models from the microscopic ones. The spectrum of methods is not yet complete, for example quantum–mechanical effects are still not properly included in the theory, and even the coupling of mechanical and electromagnetic fields has not yet been completely clarified. The development of such methods is a very active and interesting field of research (see, e.g. [57, 1, 44, 31]), which we do not discuss here.

Successful application of the general abstract methods to specific concrete model problems is a much more recent development. In the field of solid–solid phase transitions in crystals, the tools of quasiconvexity deliver sharp conditions on the compatibility of different phases, and on the possibility of finding microstructures which realize a given macroscopic average deformation [4, 13, 47]. Whereas explicit computations have been possible only in very few cases, the method has proven to have a wider field of applicability than phase transitions in crystals, see for example the work on nematic elastomers discussed below. Application of the same ideas to magnetostrictive materials has led to a simple interpretation of experimental data, which in turn furnishes the theoretical understanding needed to devise improved experimental devices [22, 58]. Even solids with simple (convex) elastic properties have a surprisingly complex behavior in nontrivial geometries. The blistering patterns of compressed thin films can be in a first approximation modelled by the scalar eikonal equation [34], and fascinating self–similar folding patterns emerge in a more refined vectorial plate theory [6, 41, 5]. The search for dimensionally reduced theories for the elasticity of thin films has attracted considerable attention for more than a century. It has been recently possible to rigorously derive, via Γ–convergence, the limiting two–

dimensional theory describing resistance to bending of an unstretched film [51, 30]. A very interesting problem which is still open is how to rigorously derive a two–dimensional theory which accounts both for bending and for stretching and provides, in a well–defined sense, an optimal approximation of the three–dimensional theory.

This paper presents two case–studies in which a mathematically rigorous result on the transition from one scale to another has led to simplified modeling, easier numerical computation, and improved understanding of the large–scale effective material behavior. Before presenting the specific examples we summarize the general approach.

- The separation of scales allows one to derive analytically a reduced (coarse–grained) problem. This is a mathematical step, based on assuming a microscopic model, and rigorously deriving the limiting macroscopic model when one parameter, representing the ratio between the micro and the macro scales, tends to zero.

- The reduced macroscopic problem can be solved numerically in a much more efficient fashion. This second step, which typically is of computational nature, requires explicit knowledge not only of the general form of the model, but also of the parameters, and allows one to compare quantitatively with experiment. Detailed understanding of the coarse–grained model and of the kind of convergence used in deriving it from the microscopic one indicates also which quantities can be computed robustly.

- From the solution of the coarse–grained problem one can gain some insight in the fine–scale structure by retracing the steps that led to its derivation. While this step is often affected by non–uniqueness of the microscropic pattern corresponding to a given macroscopic state, it can nevertheless give some heuristic understanding of the small scales, as well as valuable insight on corrections to the coarse–grained model coming from the finiteness of the small length scales.

Two specific examples where this strategy been successfully applied to the derivation of a macroscopic model from a microscopic one are soft magnetic films and nematic elastomers. In both examples, the mathematical approach has not only permitted to justify rigorously existing reduced models, but also led to a better understanding of the material behavior. For soft magnetic films the rigorous analysis led to a reduced model which extends into the regime of field penetration, and for nematic elastomers to the discovery of the "smectic" phase.

2 Soft magnetic films

Soft ferromagnetic films are of great interest both for applications and as a model physical system. Their sensitive response to applied magnetic fields makes them useful for the design of many devices, including sensors and magnetoelectronic memory elements. The presence of significant hysteresis with relatively simple domain structures, together with the availability of a wealth of experimental and numerical data, makes such films an ideal candidate for understanding the microscopic origins of magnetic hysteresis. Such phenomena are correctly described by micromagnetism, a nonlocal, nonconvex variational model which dates back to Landau and Lifshitz [43] and Brown [11], described in Section 2.1. Direct numerical simulations of micron–size specimens based on micromagnetics are however beyond the current reach of scientific computing, due to the broad spectrum of length scales which need to be resolved simultaneously (see Section 2.1). We focus on the response to weak external fields of soft films, with parameters scaling as specified in Section 2.2. Important progress in the conceptual understanding of the equilibrium patterns in such films was achieved through simplified ad–hoc models [7, 12]. These models, however, lack a variational formulation (hence hindering efficient numerical simulations) and their connection with the general theory of micromagnetism has not yet been fully understood. It is therefore unclear whether these models deliver good approximations to minimizers of the full energy, and if so in which range of material and geometric parameters this approximation is valid. The natural mathematical tool to attack these issues is Γ–convergence [19, 20, 18, 10]. In Section 2.2 we present a rigorous derivation, via Γ–convergence, of a dimensionally reduced model, and discuss in which sense the minimizers of the micromagnetic energy converge, as the film thickness tends to zero, to the solutions of the limiting problem. The Euler–Lagrange equations coming from the reduced variational problem lead to the models proposed in [7] and [12] for small fields. Numerical results are compared with experimental measurements in Section 2.3.

2.1 Micromagnetics

Ferromagnetic materials display a complex microstructure of magnetic domains, walls, Bloch lines and singular points ranging from 100 μm down to a few nm. The rich source of experimental data and the simple mathematical formulation makes the analysis of magnetic microstructures an excellent model problem to develop new mathematical tools for the understanding of multiscale problems.

Somewhat surprisingly the huge variety of magnetic structures can often

be understood through minimization of a simple energy functional, which only involves two material parameters. Let the open bounded set $\omega \subset \mathbb{R}^3$ represent a magnetic body and let $m : \omega \to \mathbb{R}^3$ denote its magnetization, which satisfies the saturation condition $|m| = 1$. For convenience we shall extend the magnetization by zero outside ω, so that $m : \mathbb{R}^3 \to \mathbb{R}^3$ satisfies $|m| = \chi_\omega$, where the characteristic function of ω is defined by $\chi_\omega(x) = 1$ if $x \in \omega$, $\chi_\omega(x) = 0$ if $x \in \mathbb{R}^3 \setminus \omega$. We now define the energy associated to such a magnetization, in suitable non–dimensional units [43, 11] (see also [36, 8]). The micromagnetic energy depends on the material parameters d and Q, which are real constants, and on the anisotropy function $\phi : S^2 \to \mathbb{R}$, which we assume to be smooth.

Definition 2.1 (Micromagnetics). *Given an open bounded set $\omega \subset \mathbb{R}^3$ (the magnetic body) function $h_{\rm ext} \in L^1(\omega, \mathbb{R}^3)$ (the external field), and a vector field $m \in L^\infty(\mathbb{R}^3, \mathbb{R}^3)$ (the magnetization), the three–dimensional micromagnetic energy is*

$$\begin{aligned} E^{(3\mathrm{D})}_{d,Q}(m, h_{\rm ext}, \omega) &= d^2 \int_\omega |\nabla m|^2 dx + Q \int_\omega \varphi(m)\, dx \\ &\quad + \int_{\mathbb{R}^3} |h_{\rm dem}|^2 dx - 2 \int_\omega h_{\rm ext} \cdot m \, dx \,, \end{aligned} \tag{2.1}$$

if $|m| = \chi_\omega$, and $+\infty$ otherwise. The demagnetizing field $h_{\rm dem} = -\nabla u$ is obtained via Maxwell's equations,

$$\mathrm{div}(-\nabla u + m) = 0 \qquad \text{in } \mathbb{R}^3 \,, \tag{2.2}$$

where the divergence is understood in the sense of distributions. The four terms in (2.1) are referred to as the exchange, anisotropy, magnetostatic and external field (or Zeeman) energy, respectively.

To the naive mathematical eye the exchange energy $|\nabla m|^2$ is the highest–order term which makes (2.1–2.2) a (nonlocal) lower–order perturbation of the harmonic map problem. While this point of view is useful to understand local properties, such as regularity of minimizers, it does not provide much insight into the complexity of the observed magnetic microstructures. Indeed much of the microstructure formation is driven by the magnetostatic energy, and the exchange energy acts primarily as a limiting factor against infinite refinement. To get a better understanding of the energy functional it is useful to look at the different energy terms separately.

- The anisotropy energy $\varphi(m)$ favors special directions of the magnetization. Most materials have either uniaxial or cubic symmetry. The

relative importance of the anisotropy term is measured by the quality parameter Q, which varies over five orders of magnitude between different materials. Materials with a low Q, where the magnetization can rotate easily, are termed *soft* ferromagnets. In the polycrystalline Permalloy thin films discussed below, the fine–scale fluctuations in the crystal orientation result in a very small effective Q. In the following we shall consider only the homogenized material, which is magnetically soft, and not discuss the grain structure further.

- The magnetostatic energy $|h_{\mathrm{dem}}|^2$ tries to eliminate the (distributional) divergence of m (see (2.2)). Written out separately for the interior and the boundary (with outer normal ν) of ω this becomes

$$\operatorname{div} m = 0 \quad \text{in } \omega \qquad\qquad m \cdot \nu = 0 \quad \text{on } \partial\omega\,. \tag{2.3}$$

  This is known as the "principle of pole avoidance". It favors a magnetization which is parallel to the boundary and in particular strongly disfavors uniform magnetization of the sample.

- The exchange energy $|\nabla m|^2$ favors uniform or at least slowly–varying magnetizations. It sets the finest length scale and the properties of the walls, which in turn influence the larger length scales.

2.2 Thin film limit

We now consider a thin film, i.e. take $\omega = \Omega \times (0,t)$ with $t \to 0$ and $|\omega|$ of order 1. Throughout this section upper–case letters denote quantities entering the reduced two–dimensional problem. We first outline the general argument to motivate the definition of the two–dimensional functional, then state our convergence result.

We consider external fields h_{ext} with vanishing out–of–plane component, which scale linearly with the thickness t, and assume that the material parameters are such that $Q \ll t$ and $t^3 \ll d^2 \ll t/\ln(1/t)$. These conditions are well satisfied in typical Permalloy films, where $Q = 2.5 \times 10^{-4}$, $t = 0.01$ and $d = 0.005$ for a typical disk with diameter 1 μm (the length units adopted here are such that $|\Omega|$ is of order 1). We remark that this range includes film thicknesses over which radically different wall types, from symmetric Néel to asymmetric Bloch, are to be expected [36].

Our Γ–convergence result is based on the heuristic observation that, in the limit $t \to 0$, a hierarchical structure emerges in the micromagnetic energy $E^{(3\mathrm{D})}$. We now discuss the scaling of the various contributions, which is summarized in Table 2.1. This will motivate our choice of the scaling of

t	m_3	magnetostatic
$d^2/t \gg t^2$	$\frac{\partial m}{\partial x_3}$	exchange
$t^2 \ln(\frac{1}{t})$	$[M \cdot \nu]$	magnetostatic
t^2	$\operatorname{Div} M$	magnetostatic
$Qt \ll t^2$	$\varphi(m)$	anisotropy
higher order	walls, Bloch lines	all energies

TABLE 2.1: Scaling of the relevant energy terms in (2.1) and their physical origin.

material parameters and the identification of the relevant energy scaling, leading to the study of the limit of $t^{-2}E^{(3D)}$.

An out–of–plane component m_3 of the magnetization of order one throughout the sample determines a magnetostatic contribution of order t. Analogously, magnetization changes along the thickness direction x_3 give rise to an exchange energy of order $d^2/t \gg t^2$. Both are of order lower than t^2, hence turn into sharp constraints in the limit. Therefore we can write $m = (M, 0)$, where $M : \Omega \to \mathbb{R}^2$ is the two–dimensional magnetization.

The component of M orthogonal to the lateral boundary $\partial\Omega$ of the film's cross section leads to a magnetostatic contribution of order $t^2 \ln \frac{1}{t}$ associated with "poles" proportional to $M \cdot \nu$, where ν is the outer unit normal to $\partial\Omega$. Precisely the same mechanism penalizes jumps $[M \cdot \nu]$ of the normal component of the magnetization across a line of discontinuity of M with normal ν. These lines of discontinuity arise by approximating domain walls as sharp interfaces, and since their energy is of order lower than t^2, they are also forbidden in the limit. This explains why in the limiting problem only in–plane magnetizations occur with discontinuity lines along which $M \cdot \nu$ does not jump (see Definition 2.2).

At order t^2 we find the magnetostatic energy due to "charges" proportional to the in–plane divergence $\operatorname{Div} M$, while anisotropy, walls, vortices, Bloch lines and cross–ties contribute only at higher order. Thus, with an external field scaling linearly with the thickness $h_{\text{ext}} = (tH_{\text{ext}}, 0)$, hence contributing the energy $-t^2 \int_\Omega H_{\text{ext}} \cdot M$, we have that, in the limit $t \to 0$, minimization of $E^{(3D)}$ within the restricted class outlined above results in an energetic competition at order t^2 between the aligning effect of H_{ext} and the demagnetizing effects due to $\operatorname{Div} M$. This motivates the following definition of the reduced energy.

Definition 2.2 (Reduced energy). *Given an open bounded set $\Omega \subset \mathbb{R}^2$ (the magnetic film) and a function $H_{\text{ext}} \in L^1(\Omega, \mathbb{R}^3)$ (the reduced external*

field), the reduced micromagnetic energy is

$$E^{(2D)}(M, H_{\rm ext}, \Omega) = \int_{\mathbb{R}^3} |H_{\rm dem}(x)|^2 dx - 2 \int_\Omega H_{\rm ext} \cdot M(x) dx \tag{2.4}$$

if the reduced magnetization $M \in L^\infty(\mathbb{R}^2, \mathbb{R}^2)$ *obeys*

$$|M| \le \chi_\Omega \,, \qquad \mathrm{Div}\, M \in H^{-1/2}(\mathbb{R}^2) \tag{2.5}$$

and $+\infty$ *otherwise. The reduced demagnetizing field* $H_{\rm dem}$ *is obtained by solving* $H_{\rm dem} = -\nabla U$, $\nabla^2 U = 0$ *outside* $\Omega \times \{0\}$, *and*

$$\left[\frac{\partial U}{\partial x_3}\right] = \mathrm{Div}\, M \qquad \text{on } \Omega \times \{0\} \tag{2.6}$$

where Div *denotes the two–dimensional divergence.*

The first condition in (2.5) corresponds to the convexification of the unit–length constraint present in the three–dimensional problem, and the second one to the requirement that the normal component of M does not jump across discontinuity lines and the boundary of Ω.

Guided by the heuristic argument illustrated above, we introduce the following notion of convergence.

Definition 2.3. *Given a sequence* $t^{(n)} \to 0$, *we say that the sequence* $\{(m^{(n)}, h^{(n)}_{\rm ext}, \Omega \times (0, t^{(n)}))\}$ *of admissible arguments for* $E^{(3D)}$ *converges to the two–dimensional limit* $(M, H_{\rm ext}, \Omega)$, *which is an admissible argument for* $E^{(2D)}$, *if*

$$\frac{1}{t^{(n)}} \int_0^{t^{(n)}} m^{(n)}(\cdot, x_3) dx_3 \rightharpoonup \begin{pmatrix} M \\ 0 \end{pmatrix} \qquad \text{in } L^2 \tag{2.7}$$

and

$$\frac{1}{t^{(n)}} h_{\rm ext} \rightharpoonup H_{\rm ext} \qquad \text{in } L^2 \,. \tag{2.8}$$

We are now ready to state the main result of this Section.

Theorem 2.4 (Γ–convergence). *Let* $\{t^{(n)}\}$, $\{d^{(n)}\}$ *and* $\{Q^{(n)}\}$ *be sequences such that*

$$t^{(n)} \to 0 \,, \qquad \left(d^{(n)}\right)^2 \frac{\ln 1/t^{(n)}}{t^{(n)}} \to 0 \,, \quad \text{and} \qquad \frac{Q^{(n)}}{t^{(n)}} \to 0 \,. \tag{2.9}$$

Then the reduced two–dimensional energy $E^{(2D)}$ *(Definition 2.2) is the* Γ*–limit of the rescaled full micromagnetic energy* $t^{-2} E^{(3D)}_{d^{(n)}, Q^{(n)}}$ *(Definition 2.1) with respect to the notion of convergence stated in Definition 2.3.*

Proof. As customary for Γ–convergence results, the proof consists of two parts. The first one is a lower semicontinuity result, ensuring that $E^{(2D)}$ evaluated at the limit of a converging sequence is less than or equal to the lower limit of the energy $E^{(3D)}$ evaluated along the sequence. The second part consists of a construction guaranteeing that $E^{(2D)}$ provides a sharp lower bound to the limiting values of $E^{(3D)}$, i.e., that for every admissible argument M of $E^{(2D)}$, there exists a sequence converging to it such that the upper limit of $E^{(3D)}$ computed along the sequence is bounded above by $E^{(2D)}(M)$. The physical intuition which builds upon Table 2.1 plays a crucial role in guiding the constructive part of the proof, which is given in [25]. □

Remark 2.5. *In the thin film limit, the unit length constraint on the magnetization vector is lost. Indeed, the non–convex constraint $|m| = \chi_\omega$ of the full magnetostatic problem is replaced by the weaker, convex constraint*

$$|M| \leq \chi_\Omega \tag{2.10}$$

in the reduced problem. This is due to the fact that, at small thicknesses, the energy cost of in–plane, divergence–free fluctuations of the magnetization vector is small (in fact, zero at order t^2).

Remark 2.6. *If the external field H_{ext} is a smooth gradient (this includes e.g. the typical case $H_{\text{ext}} = const$ on Ω), then the functional $E^{(2D)}$ depends on M only via the surface charge $\sigma = -\operatorname{Div} M$, and it is strictly convex in σ. Indeed, $\int_{\mathbb{R}^3} |H_{\text{dem}}|^2\, dx$ is a quadratic functional of σ and an integration by parts shows that $\int_\Omega H_{\text{ext}} \cdot M\, dx$ is a linear functional of σ.*

The stationary points M of the functional (2.4) satisfy the Euler–Lagrange equations

$$H_{\text{dem}} + H_{\text{ext}} = \lambda M \quad \text{and} \quad \lambda\,(1 - |M|) = 0 \tag{2.11}$$

in ω, where $\lambda(x) \geq 0$ is the Lagrange multiplier associated with the pointwise constraint $|M(x)| \leq 1$. At zero external field, minimization of (2.4) gives $H_{\text{dem}} = 0$ (pole avoidance), and hence $\operatorname{Div} M = 0$ (flux closure). This corresponds to the model proposed by van den Berg [7]. In this case, (2.11) implies $\lambda = 0$. Increasing the external field strength, one first encounters a regime in which $H_{\text{dem}} + H_{\text{ext}}$ remains zero. This is the field–expulsion regime, which corresponds to the model proposed by Bryant and Suhl [12]. At higher fields, no such solution is possible, and one obtains $\lambda > 0$, $|M| = 1$ at least in part of the domain. In these regions the magnetization M is uniquely determined by the Euler–Lagrange equation (2.11). The regions of Ω where $\lambda(x) > 0$ are those where the induced field is unable to cancel the external field (i.e., the external field penetrates the sample).

Remarks 2.5 and 2.6 indicate that the reduced problem $E^{(2D)}$, or equivalently (2.11), is a convex, quadratic problem, which can be efficiently solved numerically, obtaining a unique solution for $\mathrm{Div}\, M$ for each external field H_{ext}. Since $\mathrm{Div}\, M$ determines H_{dem} uniquely, also the regions of field penetration and the magnetization inside these regions are uniquely determined through (2.11). This would conclude the first part of our program: a simple limiting functional has been derived, which can be easily minimized numerically, and which delivers the robust quantities of the problem, namely, $\mathrm{Div}\, M$ throughout the sample, the region of field penetration, and the magnetization M *inside* this region.

We shall now move to the final part of our program, i.e., to the reconstruction of the non–robust quantities entering the original problem from the solution of the reduced one. In particular, the key quantity of interest if the magnetization M *outside* the region of field penetration.

Remark 2.7. *The set of regular in–plane vector fields of unit length and with given surface charge is large in the following sense: For any regular M_0 which obeys (2.10) there exist many regular M of unit length with the same surface charge:* $\mathrm{Div}\, M = \mathrm{Div}\, M_0$. *Indeed, we may write $M = \nabla^\perp \psi + M_0$ where $\nabla^\perp \psi = (-\partial\psi/\partial x_2, \partial\psi/\partial x_1)$ and the continuous function $\psi(x)$ on Ω solves the boundary value problem*

$$|\nabla^\perp \psi + M_0| = 1 \ \text{in}\ \Omega, \tag{2.12}$$

$$\psi = 0 \ \text{on}\ \partial\Omega. \tag{2.13}$$

Condition (2.10) ensures the existence of a solution to (2.12–2.13). One can generate many solutions by imposing the additional condition $\psi = 0$ on an arbitrary curve contained in Ω.

A selection criterion among the minimizers of (2.4) based on further minimizing suitably defined wall and Bloch line energies should emerge from an asymptotic development of the micromagnetic energy functional to order higher than two in the film thickness, but this is not attempted here (see Section 2.4).

2.3 Numerical results and comparison with experiment

The simplified structure of the two–dimensional limiting problem permits an efficient numerical solution. Minimization of $E^{(2D)}$ only delivers the divergence of M, not the full vector field. A direct experimental determination of the same quantity, for a comparison, is however difficult. Therefore, after having computed the divergence by computing one of the minimizers of

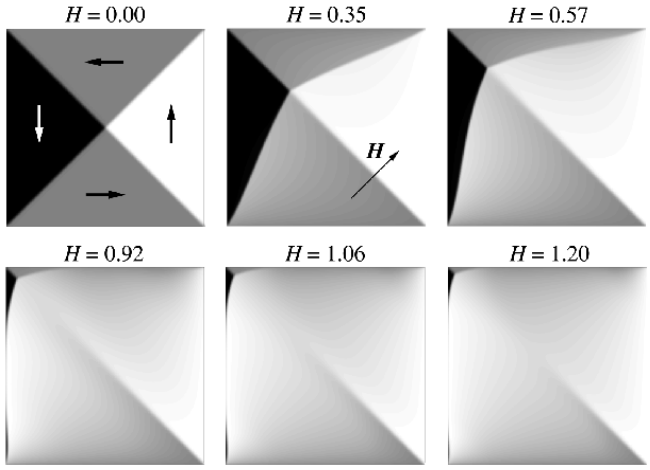

FIGURE 2.1: Numerical results: gray–scale plots of the vertical component of magnetization for different values of the external field H_{ext}. The direction of the external field is indicated by the arrow in the second plot.

$E^{(2D)}$ with length less than or equal to one, in a second step we determine a magnetization field which has unit length and the given divergence, using the heuristic selection criterion discussed below. The result is then compared with experiment.

The first computational step is a convex (though degenerate) variational problem. We solve it using an interior point method (see [27] for details). For the second step, we recall that the solution of (2.12–2.13) is not unique. However there is a unique viscosity solution (see e.g. [28]), which can be computed efficiently using the level–set method [53].

The numerical scheme above selects one of the many minimizers M. The selection principle implicit in this scheme is similar to the one proposed by Bryant and Suhl [12]. It appears to pick a minimizer with as few walls as possible. Thus it is not unlike the more physical selection mechanism of minimizing wall energy, which one can see as a higher–order correction to (2.4).

Figure 2.1 shows the predictions of our numerical scheme for a square film of edge–length one, subject to a monotonically increasing uniform field applied along the diagonal. The comparison of our predictions with the response of two Permalloy ($Ni_{81}Fe_{19}$, $J_s = 1.0$ T) square samples of edge lengths $L = 30$ and 60 μm and thicknesses $D = 40$ and 230 nm, respectively, as observed in a digitally enhanced Kerr microscope (see Figures 2.2 and 2.3) shows a very good agreement between theory and experiment.

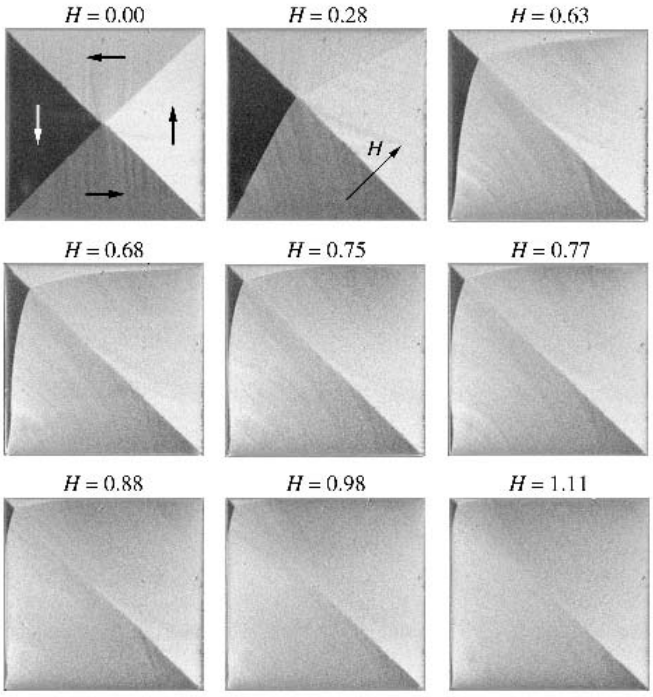

FIGURE 2.2: Observed domain patterns on Permalloy square films with side 60 μm, and thickness 230 nm. The gray–scale represents the vertical component of the magnetization. Courtesy of R. Schäfer, IFW Dresden.

2.4 Discussion

The reduced model derived in the previous sections is able to capture the experimentally observed behavior in a broad range of material and geometric parameters. It determines the micromagnetic energy to principal order, and the associated robust physical quantities that are expected to have little or no hysteresis — the charge density, the region of field penetration, and the magnetization in the penetrated region.

A natural counterpart to the broad applicability of the model is its degeneracy, which limits the predictive power. The reconstruction procedure outlined above provides a specific magnetization pattern which is consistent with experimental observations, but a rigorous mathematical justification of the selection criteria has not yet been presented. The degeneracy is strictly connected to the disappearance of the exchange energy, and to the loss of the constraint of unit length. The derivation of a model in which this degeneracy is lifted, through inclusion of higher–order corrections to the energy, will most probably involve an analysis of the domain walls. As discussed in [36],

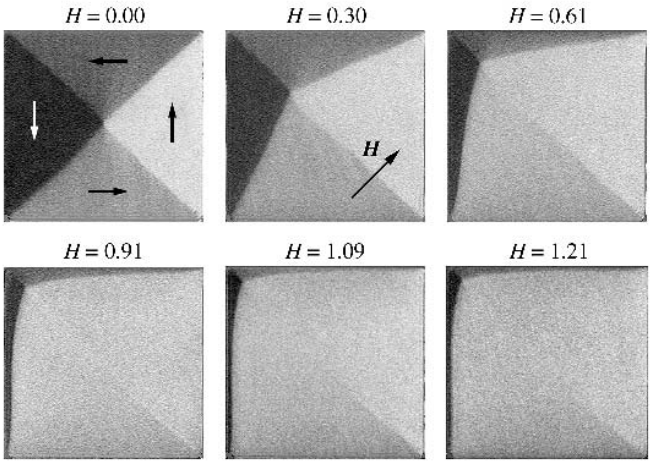

FIGURE 2.3: Observed domain patterns on Permalloy square films with side 30 μm and thickness 40 nm. Courtesy of R. Schäfer, IFW Dresden.

different wall types are expected to be present in the range of thicknesses in which our theory applies. Therefore we expect that a reduction in the degeneracy of the theory will be accompanied by a partitioning of its range of applicability into a number of separate components, each requiring a different analytic treatment. Complete results of this nature are not yet available, but progress towards overcoming some of the key obstacles has been reported. On the one hand, the structure of the Néel walls has been elucidated, including the logarithmic tails, at least for the 180° case [24, 45]. Progress on the mathematical treatment of cross–tie walls is reported in [26]. Closely related variational problems concerning energies where the higher–gradient still survives as a singular perturbation have been studied in [3, 40, 52]. The related issue of the conservation of the constraint $|M| = 1$, which mathematically is a compactness issue, has also been successfully addressed in various singularly perturbed variational problems mimicking micromagnetism [2, 23, 38, 37]. A different class of refinements of the theory presented here would aim at including hysteresis and, in general, dynamic effects. The reduction to two dimensions of the Landau–Lifshitz–Gilbert equations of micromagnetic dynamics has been addressed, for example, in [32].

3 Nematic elastomers

The elastic properties of weakly cross–linked nematic chains display in an experimentally accessible setting the fascinating consequences of the non–

quasiconvexity of an elastic energy density in nonlinear elasticity and its application to the mathematical modeling of rubber–like materials.

As first predicted by Golubović and Lubensky [35], isotropic gels prepared by cross–linking liquid polymers with a nearby nematic phase are, at least in some cases, close to a transition to an anisotropic phase, characterized by the coupling of elastic deformations to the alignment of the nematic director (see Figure 3.1). The elastic energy is in this case approximately minimized by all volume–preserving uniaxial deformations of given magnitude, independently of the orientation of the principal stretch directions [9, 59, 61]. These states form the zero set of a suitably defined microscopic energy W. Furthermore, all states with smaller stretches can be obtained by combining zero–energy states with different orientations in different parts of the domain, i.e., by using mixtures of pure states [59, 61].

The microscopic model involves therefore multiple energy–minimizing states, which can be combined on a small scale to obtain many more low–energy macroscopic deformations. In the effective macroscopic model the fine–scale oscillations are averaged out in the kinematics, but correctly accounted for in the energetics. Deducing such a macroscopic model amounts to determining the quasiconvexification of the microscopic energy. The macroscopic model, which is free from oscillations, is used to compute numerically a macroscopic deformation field. A possible microscopic representation of the macroscopic deformation is then recovered by "inverting" the quasiconvexification procedure. The organization of the following sections follows closely the mentioned line of thought. In Section 3.1 we present the derivation of the microscopic energy, whose quasiconvexification is then obtained in Section 3.2. Finite–element numerical computations are discussed in Section 3.3, together with the results on the microscopic deformation obtained with the mentioned inversion procedure. In Section 3.4 we discuss the issue of attainment, i.e. of whether structures on an infinitesimal scale in large parts of the domain are necessary in order to minimize the given energy, or if there is a configuration with the same energy where infinite refinement occurs only along the boundary, or not at all. Finally, in Section 3.5 we discuss critically our results and the validity of the adopted microscopic model.

3.1 Microscopic model

Nematic elastomers are formed by cross–linking polymeric chains which are subject to nematic ordering in a certain temperature range. Nematic ordering, which is typical of elongated, rod–like molecules, means that the rotational invariance of the isotropic liquid is broken and molecules align their axis in some direction n. In an elastomer, where the mesogens cannot spa-

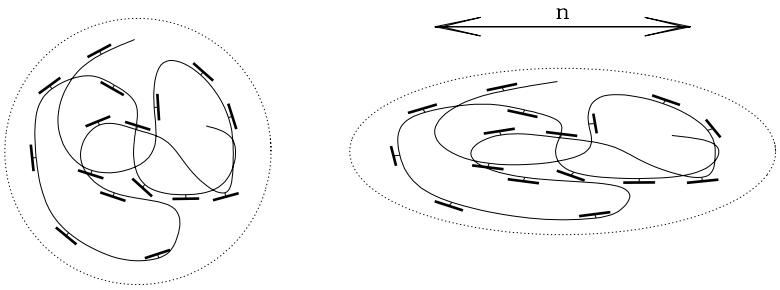

FIGURE 3.1: Schematic representation of the deformation mechanism. In the isotropic phase (left panel) the polymer can be imagined as a Gaussian coil with attached side mesogens, whose orientation is random. In the nematic phase (right panel) the mesogens have a tendency to align, and this induces a uniaxial deformation of the coil. The director n, in non–chiral liquid crystals, does not have an orientation and should therefore be identified with $-n$.

tially rearrange, the orientation process is coupled to a uniaxial deformation of the polymeric chain along n (see Figure 3.1).

Elastomeric solids are characterized by a small shear stiffness, which derives mainly from entropic effects, whereas the resistance to compression is much larger. We follow common practice and model them as incompressible materials, i.e., from now on we assume that the elastic energy density is infinite for all deformations which are not volume–preserving. The free energy which governs the response to shears can be computed from statistical mechanics. The probability distribution giving the likelihood that an isotropic polymer chain has end–to–end span described by the vector R is, in the Gaussian approximation,

$$P_{\text{isotropic}}(R) = \left(\frac{3}{2\pi L}\right)^{3/2} \exp\left(-\frac{3}{2L}|R|^2\right) , \tag{3.1}$$

where L is a measure of the the length of the polymer chains. Assume now that the polymer network is affinely deformed, and let F be the deformation gradient. The corresponding elastic free energy, of entropic nature, is obtained by averaging the logarithm of $P_{\text{isotropic}}(FR)$ with respect to $P_{\text{isotropic}}(R)$, i.e.

$$W_{\text{isotropic}}(F) = -k_B T \langle \ln P_{\text{isotropic}}(FR) \rangle_{P_{\text{isotropic}}(R)} = \frac{1}{2} k_B T |F|^2 + c \tag{3.2}$$

and corresponds to the standard neo–hookean elasticity of rubber. In (3.2) and below, c denotes a constant which does not depend on F, and hence has no effect on the elastic properties and can be safely ignored. Similarly, since we will be working at constant temperature, the Boltzmann factor $k_BT/2$ will be dropped in what follows.

In nematic elastomers, the chains have a preferred orientation, since extension parallel to n is more likely than in other directions. More precisely, one gets

$$P_n(R) = \left(\frac{3}{2\pi L}\right)^{3/2} \exp\left(-\frac{3}{2L} R_i (U_n^{-2})_{ij} R_j\right) \tag{3.3}$$

where

$$U_n = a^{1/6}\left[\mathrm{Id} + (a^{-1/2} - 1) n \otimes n\right] \tag{3.4}$$

corresponds to a uniaxial stretch along n. The coefficient $a \in (0,1)$ measures the effect of local ordering on the elastic properties, and clearly the isotropic case is recovered for $a = 1$ (this corresponds either to zero nematic ordering, or to zero coupling between the nematic ordering and the elastic deformation). Let n_0 denote the value of n at cross–linking, which we assume to be done in a perfectly ordered state, i.e. with n_0 and a constant across the sample (effects of weak disorder in the cross–linking configuration will be discussed in Section 3.5). We are interested in the elastic properties of the material after cross–linking. Since the chain distribution in the melt has been frozen, the probability distribution remains P_{n_0}. The free energy at given director n and deformation gradient $\tilde{F}$ is then obtained by the quenched average

$$\begin{aligned} \tilde{W}_{\mathrm{BTW}}(\tilde{F}, n) &= -k_BT \langle \ln P_n(\tilde{F}R) \rangle_{P_{n_0}(R)} \\ &= \frac{1}{2} k_BT \,\mathrm{Tr}\, U_n^{-2} \tilde{F} U_{n_0}^2 \tilde{F}^T + c \\ &= \frac{1}{2} k_BT \,\mathrm{Tr}\, U_n^{-2} (\tilde{F} U_{n_0})(\tilde{F} U_{n_0})^T + c\,. \end{aligned} \tag{3.5}$$

The energy (3.5) was first obtained by Bladon, Terentjev and Warner (BTW) in [9]. Using this energy BTW predicted soft elastic response and microstructure (stripe domains) originating from the non–quasiconvexity of W_{BTW}; such predictions have been verified experimentally [42]. However, the experimental results do not show ideally soft response, but rather exhibit both a stress threshold and a small resistance at small stretches, on a scale much smaller than k_BT but still measurable. This observation led to a theoretical search for corrections to (3.5), the main candidates being higher gradient energies (penalizing sharp changes in the director direction n) and disorder in the

cross–linking configuration. Various corrections to $W_{\rm BTW}$ have been proposed in the literature [59, 62, 29, 60] and will be discussed in Section 3.5 below. The last expression in (3.5) emphasizes the high symmetry of the problem which can be obtained by choosing as reference configuration the stress–free state of the ideal isotropic "high–temperature" phase, which differs from the actual cross–linking configuration by a uniaxial stretch U_{n_0}. From now on we consider the strain with respect to this new reference configuration, $F = \tilde{F}U_{n_0}$. Choosing $k_BT/2$ as energy units, and adding a suitable constant, one gets

$$W_{\rm BTW}(F,n) = \operatorname{Tr} U_n^{-2} F F^T - 3 = a^{-1/3}\left[|F|^2 - (1-a)|F^T n|^2\right] - 3 \quad (3.6)$$

for volume–preserving deformations F, and infinity if $\det F \neq 1$.

Minimizing locally over unit vectors n corresponds to replacing $|F^T n|$ with the largest singular value of F. Indeed, due to the full rotational symmetry of this problem, the energy can only depend on the singular values of F, which we denote by $\lambda_1 \leq \lambda_2 \leq \lambda_3$ (their squares are the eigenvalues of F^TF and FF^T). One then gets

$$W_{\rm ne}(F) = \begin{cases} a^{-1/3}\lambda_1^2(F) + a^{-1/3}\lambda_2^2(F) + a^{2/3}\lambda_3^2(F) - 3 & \text{if } \det F = 1 \\ +\infty & \text{else} \end{cases} \quad (3.7)$$

which constitutes the starting point of our analysis.

We first present a simple argument which illustrates, in a special case, the origin of the experimentally–observed stripe domains from an energetic point of view. Consider a macroscopic deformation gradient $F = \operatorname{diag}(a^{1/6}, \mu, a^{-1/6}/\mu)$, with $a^{1/6} < \mu < a^{-1/3}$. By definition, $W_{\rm ne}(F) > 0$, but one can find a sequence of zero–energy deformations which converge (weakly in $W^{1,2}$) to $u(x) = Fx$. The construction uses a decomposition of the domain in equally spaced layers in which the deformation gradient takes the values

$$F_\pm = F \pm \delta e_2 \otimes e_3 = \begin{pmatrix} a^{1/6} & 0 & 0 \\ 0 & \mu & \delta \\ 0 & 0 & a^{-1/6}/\mu \end{pmatrix} \quad (3.8)$$

where δ is chosen so that $W_{\rm ne}(F_\pm) = 0$. A short calculation shows that this is possible if and only if $a^{1/6} \leq \mu \leq a^{-1/3}$. We emphasize that it is possible to find a Lipschitz function whose gradient only takes the values F_+ and F_- precisely because $F_+ - F_-$ is a rank–one matrix. The boundary of the region where the gradient equals F_+ has normal e_3 (see Figure 3.2). It can be expected that for some deformation gradients more complicated constructions can lead to smaller energy than the one obtainable by a simple laminate.

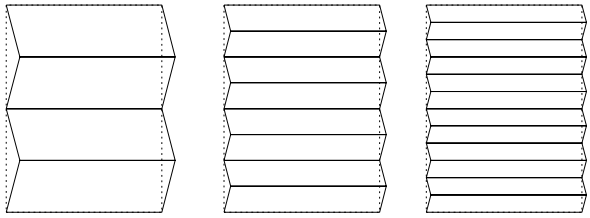

FIGURE 3.2: Approximation of an affine deformation by a sequence of oscillating functions (see text).

Indeed, we will prove below that a second iteration of the above construction is always optimal for this energy (Theorem 3.1), and then characterize the set of matrices F where a single iteration is sufficient (Theorem 3.3).

3.2 Quasiconvexification

In this section we give a mathematical formulation of the foregoing constructions. We start with some definitions. We say that a probability measure on 3×3 matrices $\nu = \mu_1 \delta_{F_1} + \mu_2 \delta_{F_2}$ is a first–order laminate with average F if $\mu_1 F_1 + \mu_2 F_2 = F$ and $\mathrm{rank}(F_1 - F_2) = 1$. Here δ_F denotes a Dirac delta concentrated on the matrix F. Laminates of order k with average F are then defined as the set of probability measures obtained from laminates of order $k-1$ replacing any δ_{F_j} with a first–order laminate with average F_j. We have seen above that laminates offer a natural way to reduce the energy by using complex deformation patters. The optimal energy which can be obtained with laminates is called the lamination convex envelope, and is defined as $\phi^{lc}(F) = \inf\langle \phi, \nu \rangle$, where the infimum is taken over all laminates with average F (we denote by ϕ a generic energy density, and use W for the specific expressions which concern nematic elastomers).

Laminates are very useful but also very special constructions, and it is therefore natural to ask whether other constructions can further reduce the energy. The optimal result is the quasiconvex envelope, defined by

$$\phi^{qc}(F) = \inf_{y \in W^{1,\infty}} \left\{ \frac{1}{|\Omega|} \int_\Omega \phi(\nabla y(x)) dx : y(x) = Fx \text{ on } \partial\Omega, \det \nabla y(x) = 1 \right\} . \tag{3.9}$$

It turns out that for the case of interest here $\phi^{qc} = \phi^{lc}$ and second–order laminates are sufficient. In order to better elucidate the mathematical

structure of the problem, we consider a generalization of the above energy,

$$W(F) = \begin{cases} \left(\frac{\lambda_1(F)}{\gamma_1}\right)^p + \left(\frac{\lambda_2(F)}{\gamma_2}\right)^p + \left(\frac{\lambda_3(F)}{\gamma_3}\right)^p - 3 & \text{if } \det F = 1 \\ +\infty & \text{else} \end{cases} \tag{3.10}$$

where $\gamma_1 \leq \gamma_2 \leq \gamma_3$ are given positive constants, with $\gamma_1\gamma_2\gamma_3 = 1$ and $p \geq 2$. The energy (3.7) of nematic elastomers is recovered by choosing $p = 2$, $\gamma_1 = \gamma_2$. The energy W is nonnegative, and it vanishes only for matrices F which have singular values $(\gamma_1, \gamma_2, \gamma_3)$, i.e.

$$W(F) = 0 \text{ iff } F \in SO(3)\text{diag}(\gamma_1, \gamma_2, \gamma_3)SO(3)\,. \tag{3.11}$$

The quasiconvexification of W has been obtained by DeSimone and Dolzmann in [21], and later extended by Šilhavý in [54].

Theorem 3.1 ([21]). *Let W be given by (3.10). Then,*

$$W^{\text{qc}}(F) = \begin{cases} \tilde{g}(\lambda_3(F), \lambda_1^{-1}(F)) & \textit{if } \det F = 1 \\ +\infty & \textit{else} \end{cases} \tag{3.12}$$

where $\tilde{g} : (0,\infty)^2 \to \mathbb{R}$ is the convex nondecreasing function given in (3.19).

Proof. The proof is based on constructing a polyconvex function which lies below W, and therefore gives a lower bound to W^{qc}, and comparing with upper estimates obtained by constructing laminates. Here we outline the main ideas, using a slight variant of the original argument.

We first describe in general our strategy for evaluating the quasiconvex envelope of a function ϕ. The starting point is to obtain good candidates for the polyconvex envelope ϕ^{pc}, which is the largest polyconvex function less than or equal to ϕ. Recall that a function $\phi : \mathbb{R}^{3\times 3} \to \mathbb{R}$ is polyconvex if there exists a convex function $h : \mathbb{R}^{19} \to \mathbb{R}$ such that $\phi(F) = h(F, \text{cof } F, \det F)$, and that $\phi^{pc} \leq \phi^{lc}$. Given finitely many polyconvex functions $\{z_i\}$, all functions ϕ such that $\phi(F) = \eta(\{z_i(F)\})$, with η convex and nondecreasing in its arguments, are also polyconvex. An appropriate set of variables $\{z_i\}$ may be suggested by the structure of the problem. If one can write $\phi(F) = \eta(\{z_i(F)\})$, the largest convex and nondecreasing function $\tilde{\eta}$ less than or equal to η provides a polyconvex function $\tilde{\phi}(F) = \tilde{\eta}(\{z_i(F)\})$ not larger than $\phi(F)$, which is a lower bound for the quasiconvexification ϕ^{qc}. If one can further show that $\phi^{lc}(F) \leq \tilde{\phi}(F)$, then $\tilde{\phi}$ is the polyconvex and lamination convex envelope of ϕ. Finally, due to a result by Müller and Šverák [48], $\tilde{\phi}$ is also the quasiconvex envelope of ϕ.

We now apply this general strategy to our specific problem. Since the function

$$\psi(F) = \chi_1(\det F)\,, \qquad \chi_1(x) = \begin{cases} 0 & \text{if } x = 1 \\ +\infty & \text{else} \end{cases} \tag{3.13}$$

is polyconvex, $W^{\mathrm{qc}}(F)$ is infinite unless $\det F = 1$. Therefore we only need to consider matrices with determinant equal to one. Due to its full rotational symmetry, the energy $W(F)$ only depends on the singular values of F, which are the natural variables in which the problem should be cast. These can in turn be expressed in terms of convex functions of F and $\operatorname{cof} F$, hence of polyconvex functions of F. Indeed, the largest singular value is given by

$$s(F) = \lambda_3(F) = \max_{|e|=1} |Fe| \tag{3.14}$$

and is therefore a convex function of F. The inverse of the smallest can be written as

$$t(F) = \frac{1}{\lambda_1(F)} = \max_{|e|=1} |\operatorname{cof} Fe| \tag{3.15}$$

and is a convex function of $\operatorname{cof} F$. The intermediate singular value is then recovered by the volume constraint, $\lambda_2 = t/s$. We thus write $W(F) = g(s(F), t(F))$, where $g : (0,\infty)^2 \to \mathbb{R}$ is given by

$$g(s,t) = \left(\frac{1}{t\gamma_1}\right)^p + \left(\frac{t}{s\gamma_2}\right)^p + \left(\frac{s}{\gamma_3}\right)^p - 3\,. \tag{3.16}$$

By computing the Hessian matrix one can easily see that g is convex in s and t, however it is not increasing. More precisely,

$$\frac{\partial g}{\partial s} = p s^{p-1}\gamma_3^{-p} - p t^p s^{-p-1}\gamma_2^{-p} \tag{3.17}$$

is nonnegative if and only if $s^2 \geq t\gamma_3/\gamma_2$, and

$$\frac{\partial g}{\partial t} = p t^{p-1} s^{-p}\gamma_2^{-p} - p t^{-p-1}\gamma_1^{-p} \tag{3.18}$$

is nonnegative if and only if $t^2 \geq s\gamma_2/\gamma_1$. The significance of these conditions is best understood with reference to Figure 3.3. The range of s and t (as functions of F, with $\det F = 1$) is given by $0 < 1/t < t/s < s$, and it corresponds to the region between the two thick parabolas. The internal region between the two thin parabolas, denoted by S, is the one where both derivatives are positive. In the region I_1 we have $\partial_s g < 0$, and therefore the largest nondecreasing function below g is given by g evaluated on the common

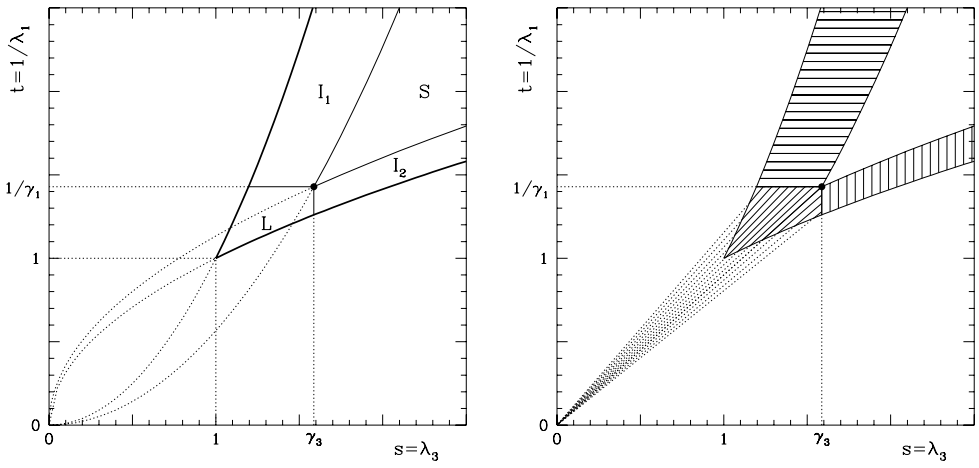

FIGURE 3.3: The phase diagram for the relaxed energy. The left panel shows the different phases and phase boundaries (see Eq. (3.19)). The right panel shows the rank–one directions in the phase diagram which correspond to keeping one singular value fixed. First the energy in the regions I_1 and the I_2 is constructed, by taking the value on the boundary with S (at fixed t in I_1, at fixed s in I_2). The construction in L is done by continuing from the boundaries of I_1 and I_2 along lines of constant $\lambda_2 = t/s$.

boundary between I_1 and S, i.e. $\tilde{g}(s,t) = g((t\gamma_3/\gamma_2)^{1/2}, t)$. Analogously in the region I_2 we get $\tilde{g}(s,t) = g(s, (s\gamma_2/\gamma_1)^{1/2})$. Finally, since $g(\gamma_3, 1/\gamma_1) = 0$ (and $g \geq 0$ everywhere), in the whole region L we get $\tilde{g} = 0$. We conclude that the highest nondecreasing function below g is given by

$$\tilde{g}(s,t) = \begin{cases} g(s,t) & \text{in S, i.e. } s^2 \geq t\gamma_3/\gamma_2 \text{ and } t^2 \geq s\gamma_2/\gamma_1 \\ 2\left(\dfrac{t}{\gamma_2\gamma_3}\right)^{p/2} + \left(\dfrac{1}{\gamma_1 t}\right)^p - 3 & \text{in } I_1\text{, i.e. } t \geq 1/\gamma_1 \text{ and } t \geq s^2\gamma_2/\gamma_3 \\ 2\left(\dfrac{1}{s\gamma_1\gamma_2}\right)^{p/2} + \left(\dfrac{s}{\gamma_3}\right)^p - 3 & \text{in } I_2\text{, i.e. } s \geq \gamma_3 \text{ and } s \geq t^2\gamma_1/\gamma_2 \\ 0 & \text{in L, i.e. } s \leq \gamma_3 \text{ and } t \leq 1/\gamma_1\,. \end{cases} \tag{3.19}$$

One can then easily check that $\tilde{g}$ is still convex (see [21] for details), and therefore $\tilde{\phi} = \tilde{g}(s(F), t(F))$ is polyconvex and it provides a lower bound for the quasiconvex envelope of W.

We now show that this bound is optimal, i.e. that the same energy can be reached by laminates. Again, the special choice of variables s and t makes the computation easy. Indeed, by rotational invariance it suffices to consider only diagonal matrices. Fix $F = \mathrm{diag}(\mu_1, \mu_2, \mu_3)$, and consider

$F_\delta = F + \delta e_1 \otimes e_2$. The matrices F_δ have $\det F_\delta = 1$, μ_3 as a singular value, and $|F_\delta|^2 = |F|^2 + \delta^2$. Let (ξ_1, ξ_2, μ_3) be the singular values of F_δ. Since $\xi_1^2 + \xi_2^2 = \mu_1^2 + \mu_2^2 + \delta^2$ and $\xi_1\xi_2\mu_3 = 1$, it is clear that by choosing a suitable δ one can reach a given pair (ξ_1, ξ_2) if and only if $|\xi_1 - \xi_2| \geq |\mu_1 - \mu_2|$, and the determinant constraint $\xi_1\xi_2\mu_3 = 1$ is satisfied. Then F is the average of a first–order laminate supported on $F_{\pm\delta}$, and $\phi^{lc}(F) \leq \phi(F_\delta) = \phi(F_{-\delta})$. Therefore in the (s,t) plane one can construct laminates along lines which keep one singular value constant, i.e. lines parallel to each coordinate axis, and lines which go through the origin as shown in Figure 3.3. The right panel shows the paths used to construct optimal laminates: constant s lines inside I_1, constant t lines inside I_3, and constant s/t lines inside L. Since the line segments used in L have one end point on the common boundary with I_1, I_3 and since these points already represent laminates, the resulting construction in L is a second–order laminate. This concludes the proof that $W^{lc} = W^{pc}$. The fact that the quasiconvex envelope also coincides with them requires a delicate treatment of the volume constraint, for which we refer to [21]. □

Remark 3.2. *For $p = 2$ and $\gamma_1 = \gamma_2 = a^{1/6}$, the relevant case for nematic elastomers, phase I_2 is absent, and (3.19) reduces to*

$$\tilde{g}(s,t) = \begin{cases} \dfrac{a^{-1/3}}{t^2} + \dfrac{a^{-1/3}t^2}{s^2} + a^{2/3}s^2 - 3 & \text{in } S, \text{ i.e. } s^2 \geq ta^{1/2} \\ 2a^{1/6}t + \dfrac{a^{-1/3}}{t^2} - 3 & \text{in } Sm, \text{ i.e. } t \geq a^{1/6} \text{ and } t \geq a^{1/2}s^2 \\ 0 & \text{in } L, \text{ i.e. } t \leq a^{1/6} \end{cases} \tag{3.20}$$

(see also Figure 3.7 below). We name Sm ("Smectic") the intermediate phase I_1 due to its peculiar mechanical behavior (see [14]).

In the construction above we used first laminates for I_1 and I_3, and second laminates for L. A natural question, which was posed and only partially answered in [21], is to ask whether the second laminates are really needed inside L. The following theorem gives a characterization of the set of gradients where first laminates are sufficient.

Theorem 3.3. *Let F be a matrix in phase L, i.e. such that $\gamma_1 \leq \lambda_1(F) \leq \lambda_3(F) \leq \gamma_3$. There is a first–order laminate with average F supported on the set $\{W(F) = 0\}$ if and only if*

$$\lambda_1(F) \leq \gamma_2 \leq \lambda_3(F)\,. \tag{3.21}$$

Proof. If F can be obtained as a simple laminate, we can write $F = M + a \otimes b$, with $W(M) = 0$. By rotational invariance we can assume M to be diagonal,

and since it has zero energy $M = \mathrm{diag}(\gamma_1, \gamma_2, \gamma_3)$. We use an extension of the argument given in [21] for the $\gamma_1 = \gamma_2$ case, and consider a unit vector v orthogonal to e_3 and to b. Then $Fv = Mv$, but since v is a linear combination of e_1 and e_2, $|Mv| \le \gamma_2$, it follows that

$$\lambda_1(F) = \min_{|n|=1} |Fn| \le |Fv| = |Mv| \le \gamma_2 \,. \tag{3.22}$$

Analogously, taking w as a unit vector orthogonal to e_1 and b, we get $\gamma_2 \le \lambda_3(F)$. This concludes the proof of the first implication.

It remains to show that every matrix in phase L obeying (3.21) can be obtained as a first–order laminate supported on zero–energy matrices. Consider $F = \mathrm{diag}(\mu_1, \mu_2, \mu_3)$ with $\gamma_1 \le \mu_1 \le \mu_2 \le \mu_3 \le \gamma_3$. The matrices

$$F_\delta = F + \delta(e_1 \cos\theta + e_3 \sin\theta) \otimes e_2 = \begin{pmatrix} \mu_1 & \delta\cos\theta & 0 \\ 0 & \mu_2 & 0 \\ 0 & \delta\sin\theta & \mu_3 \end{pmatrix} \tag{3.23}$$

all have unit determinant. The matrix F_δ has singular values $(\gamma_1, \gamma_2, \gamma_3)$ if and only if the two conditions $\mathrm{Tr}\, F_\delta^T F_\delta = \sum_i \gamma_i^2$, $\mathrm{Tr}\,\mathrm{cof}\, F_\delta^T \,\mathrm{cof}\, F_\delta = \sum_i \gamma_i^{-2}$ are satisfied. Equivalently,

$$\sum_i \mu_i^2 + \delta^2 = \sum_i \gamma_i^2 \tag{3.24}$$

and

$$\sum_i \mu_i^{-2} + \delta^2(\mu_3^2 \cos^2\theta + \mu_1^2 \sin^2\theta) = \sum_i \gamma_i^{-2} \,. \tag{3.25}$$

The first equation can always be solved for δ. The second one can then be solved for θ provided that

$$\mu_1^2 \le \frac{\sum \gamma_i^{-2} - \sum \mu_i^{-2}}{\sum \gamma_i^2 - \sum \mu_i^2} \le \mu_3^2 \,. \tag{3.26}$$

The first inequality is equivalent to

$$0 \le -\mu_1^2 \sum_i \gamma_i^2 + \sum_i \gamma_i^{-2} + \mu_1^4 - \mu_1^{-2} = \mu_1^{-2} \prod_i (\mu_1^2 - \gamma_i^2) \,, \tag{3.27}$$

which in turn gives $\mu_1 \le \gamma_2$. Analogously, the second inequality gives $\mu_3 \ge \gamma_2$. □

Remark 3.4. *For $\gamma_1 = \gamma_2$, the relevant case for nematic elastomers, the condition (3.21) is equivalent to $\lambda_1(F) = \gamma_1$. In turn, this indicates that first laminates are sufficient in phase Sm, up to the boundary with L, whereas second laminates are needed inside L.*

3.3 Finite–element computations

In this section we present our numerical computations with the quasiconvexified energy $W^{\rm qc}$ on a model problem, whose geometry and material parameters correspond to experiments reported in the literature. The loading process consists in stretching in a direction orthogonal to the director at cross–linking $n_0 = e_3$ a thin, flat rectangular sheet of size $l_1 \times l_2 \times l_3$. In our numerical simulations, we choose a typical value $a = 0.5$, which gives a spontaneous stretch $a^{-1/3} = 1.26$. Moreover we considered a fixed thickness $l_1 = 0.1 l_3$ and an aspect–ratio $l_2/l_3 = 3$ (we also performed simulations with $l_2/l_3 = 1$, see below). Lengths are here measured in the reference configuration, which is the stress–free configuration of the high–temperature phase described by $a = 1$ [this corresponds to the change of variables mentioned before (3.6)]. The initial configuration is the stress–free one (in the low temperature phase, i.e. for $a = 0.5$) with director parallel to $n_0 = e_3$, hence it is deformed with respect to the reference configuration by the affine uniaxial strain U_{e_3}. The aspect ratio in the initial configuration is thus $3a^{1/2} \sim 2.12$. In the experiment, the two faces orthogonal to e_2 are glued to two pieces of rigid material (clamps), which are then pulled away from each other. In our simulation, on those faces we impose Dirichlet boundary conditions. The stretch s is the distance between the clamps (in direction 2) in units of its initial value. We always work with zero tractions on the unclamped part of the boundary. Computations have been performed on a SUN workstation by implementing a user–defined constitutive law in a commercial finite–element software package (ABAQUS). The high degeneracy of the energy (especially in phase L, see below) requires inclusion of a small regularizing perturbation. Details of the numerical procedure and of the regularization have been described in [14].

Figure 3.4 shows the reactive force exerted by the clamps plotted against the imposed displacements. These results show the existence of a "window" of liquid–like behavior, where the force is zero within the resolution of our simulation. We shall prove later (Theorem 3.7) that, at least in a smaller window, the energy (and hence the reaction force) is exactly zero.

Several experiments [42, 64] report formation of microstructures in the central part of the sample. This is explained by the fact that, in this region, the energy is reduced by forming small–scale oscillatory patterns with alternating shears, as discussed at the end of Section 3.1. To identify the part of the sample where this happens, we plot the so–called microstructure index

$$\mathrm{I_M} = \frac{1}{\lambda_1} - a^{1/2}\lambda_3^2 \tag{3.28}$$

which is positive in phases L and Sm, and negative in phase S. Hence, $\mathrm{I_M} > 0$

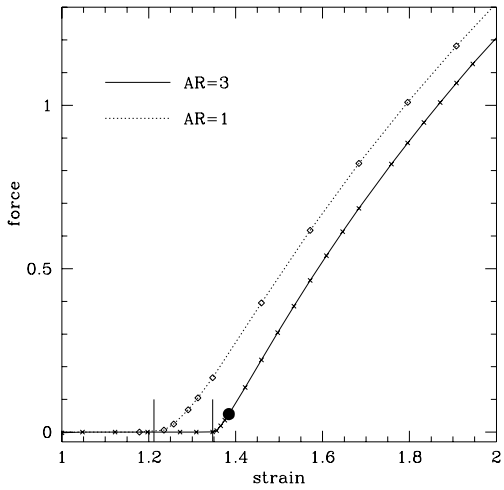

FIGURE 3.4: Force versus strain curve (crosses joined by the full line). The diamonds joined by the dotted curve are results obtained for aspect–ratio 1 (i.e. $l_2 = l_3$). The black dot marks the configuration which is presented in more detail below. The two vertical lines mark the boundary of the liquid phase as obtained with the analytic construction in Theorem 3.7.

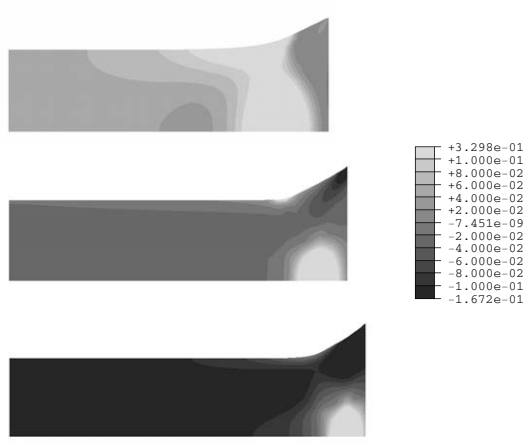

FIGURE 3.5: Plot of the microstructure index I_M for different stretches. From top to bottom, $s = 1.31$, $s = 1.38$, and $s = 1.46$. Only the quarter of the sample in the first quadrant is plotted, the rest is symmetric. The clamped boundary is the one on the right side in this figure, the lower–left corner represents the center of the sample.

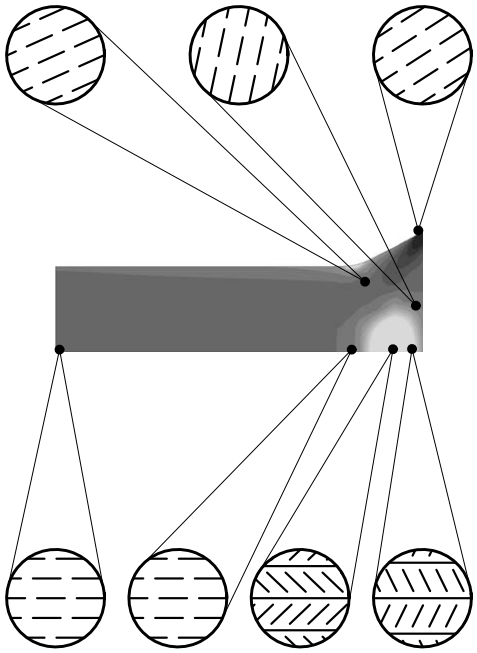

FIGURE 3.6: Microstructure index I_M and resolution in microstructures at stretch 1.38.

characterizes regions where the macroscopic deformation is achieved by a mixture of different microscopic deformations. Figure 3.5 shows a density plot of I_M for different stretches. The striking result is that a region exhibiting microstructure survives even at large stretches, around the mid–point of the boundary. We now discuss in more detail the results for a representative value of the stretch ($s = 1.38$, see the central panel of Figure 3.5 for the resulting deformation).

In Figure 3.6 we show a possible resolution of the deformation gradient using first–order laminates (as done in the construction described in Section 3.2). We choose rank–one connected matrices $F_\pm$ such that $(F_+ + F_-)/2$ agrees with the local in–plane macroscopic deformation. The "sticks" in the figures indicate the local orientation of the nematic director n, and have been obtained by plotting the eigenvector of $F_+F_+^T$ corresponding to the largest eigenvalue, i.e. the largest one among all vectors F_+e with $|e| = 1$. As was clear from the previous figures, microstructure is present only in the white region around the central part of the clamp. Indeed, the director n equals e_3 close to the clamp, whereas it equals e_2 in the center of the sample. The microstructure covers the intermediate regime. Finally, in Figure 3.7 we display the distribution in the phase diagram of the points explored by the

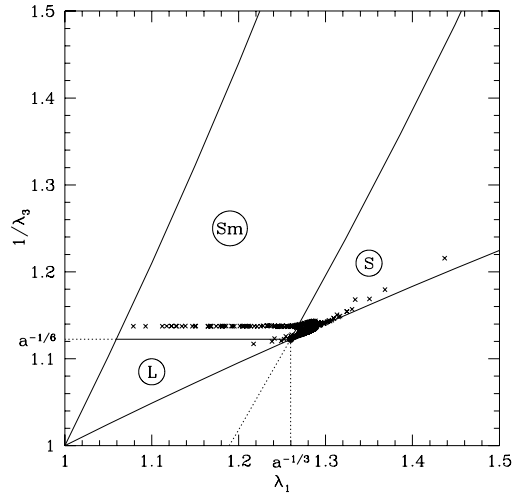

FIGURE 3.7: Macroscopic phase diagram and phase distribution at $s = 1.38$. The three regions are defined in Remark 3.2. Only the region $\lambda_3^2 \geq 1/\lambda_1 \geq \lambda_3^{1/2}$ can be attained (due to the volume constraint).

numerically computed macroscopic deformation gradient. The row of points in phase Sm corresponds to the white region in the previous figures.

3.4 Attainment results

The mathematical analysis of the microscopic energy of nematic elastomers allows one to understand and to reproduce in numerical simulations experimentally observed microstructures. The success of this approach motivates a further investigation of the mathematical origin of such microstructures. In particular, we consider two paradigmatic boundary–value problems, namely, affine Dirichlet conditions in Section 3.4.1 and the mixed boundary conditions which mimic the experimental setup in Section 3.4.2. The implications of these results on the understanding of experiments on nematic elastomers are then discussed in Section 3.5.

3.4.1 Attainment and non–attainment for Dirichlet boundary conditions

In this section we discuss the question of whether there exist Lipschitz functions u with affine boundary conditions $u(x) = Fx$ and with zero microscopic

energy, i.e. whether for a given F such that $W^{\mathrm{qc}}(F) = 0$ the infimum

$$\inf_{y \in W^{1,\infty}} \left\{ \frac{1}{|\Omega|} \int_\Omega W(\nabla y(x)) dx : y(x) = Fx \text{ on } \partial\Omega, \det \nabla y(x) = 1 \right\}, \quad (3.29)$$

which is zero by the definition of W^{qc}, is in fact attained [W was defined in (3.10)]. The answer only depends on the singular values of F, and not on the domain Ω. This issue was first investigated by Dacorogna and Tanteri in [17]. We give here an independent, complete characterization of the attainment set, based on a general construction by Müller and Šverák.

Theorem 3.5. *Let F be in the phase L, i.e.*

$$\gamma_1 \leq \lambda_1(F) \leq \lambda_3(F) \leq \gamma_3 \,, \quad (3.30)$$

and such that $W(F) > 0$. Then the infimum in (3.29) is attained if and only if $\gamma_1 < \lambda_1(F)$ and $\lambda_3(F) < \gamma_3$.

Proof. By rotational invariance, we may assume that F is a diagonal matrix, $F = \mathrm{diag}(\mu_1, \mu_2, \mu_3)$, with $\mu_1 \leq \mu_2 \leq \mu_3$. We first show that the infimum is not attained if $\mu_3 = \gamma_3$. Suppose otherwise. Then there exists a Lipschitz map u with $W(\nabla u) = 0$ a.e., and $u = Fx$ on $\partial(0,1)^3$. Then,

$$\gamma_3 = \int_{(0,1)^3} e_3 \cdot \nabla u e_3 \, dx \leq \int_{(0,1)^3} \lambda_3(\nabla u) \, dx = \gamma_3 \quad (3.31)$$

Therefore equality holds in this chain of inequalities, and since $|(\nabla u)e_3| \leq \lambda_3(\nabla u) = \gamma_3$ we get $(\nabla u)e_3 = \gamma_3 e_3$. It follows that

$$u(x_1, x_2, x_3) = F(x_1, x_2, 0)^T + \gamma_3 x_3 e_3 = Fx \quad (3.32)$$

Hence $W(\nabla u) = W(F) > 0$, a contradiction. If instead $\mu_1 = \gamma_1$, we need to consider the cofactor matrix, which like the gradient itself is a null Lagrangian. Therefore its integral depends only on the boundary values, and

$$\frac{1}{\gamma_1} = \int_{(0,1)^3} e_1 \cdot (\mathrm{cof}\, \nabla u) e_1 \, dx \leq \int_{(0,1)^3} \lambda_1^{-1}(\nabla u) \, dx \leq \frac{1}{\gamma_1} \quad (3.33)$$

so that we can conclude as before.

To prove attainment in the case $\gamma_1 < \mu_1 \leq \mu_3 < \gamma_3$, we use a special case of a more general theorem by Müller and Šverák [48], which is stated below in Theorem 3.6. In our application, K is given by $K = SO(3)\mathrm{diag}(\gamma_1, \gamma_2, \gamma_3)SO(3)$, and we only need to construct an in–approximation with $F \in U_1$. In order to do so, we choose

$$U_1 = \{F : \det F = 1, \gamma_1 < \lambda_1(F) \leq \lambda_3(F) < \gamma_3\} \quad (3.34)$$

and we define iteratively

$$U_{i+1} = U_i \bigcap \left\{ F : \lambda_1(F) < \gamma_1 + \frac{1}{i}, \lambda_3(F) > \gamma_3 - \frac{1}{i} \right\} . \tag{3.35}$$

The only thing that remains to be checked is that U_i is contained in the rank–one convex hull of U_{i+1}. This is however an immediate consequence of our construction in Section 3.2. □

Before concluding this Section, we state the result regarding the constraint $\det F = 1$ which has been used in the construction above.

Theorem 3.6 ([48]). *Let $\Sigma = \{F \in M^{3\times 3} : \det F = 1\}$, and let K be a subset of Σ. Suppose that U_i is an in–approximation of K, i.e. the U_i are open in Σ, uniformly bounded, U_i is contained in the rank–one convex hull of U_{i+1}, and U_i converges to K in the following sense: if $F_i \in U_i$ and $F_i \to F$, then $F \in K$. Then, for any $F \in U_1$ there exists a Lipschitz solution of the partial differential inclusion*

$$\begin{aligned} Du &\in K \qquad \text{a.e. in } \Omega \\ u(x) &= Fx \qquad \text{on } \partial\Omega . \end{aligned}$$

3.4.2 Attainment for a Dirichlet–Neumann problem

We now explore the attainment question for the experimentally relevant case of Dirichlet boundary conditions prescribed only on two opposite faces of a thin rectangular sheet. We will show that, for a large range of imposed stretches, zero energy can be attained by deformations whose gradients take only finitely many values.

Theorem 3.7. *The problem*

$$W(\nabla u) = 0 \text{ a.e.}, \qquad u(x) = \operatorname{diag}(\gamma_1, t\gamma_2, \gamma_3)x \text{ for } x_2 = \pm l_2 \tag{3.36}$$

has a piecewise affine solution in $\Omega = (-l_1, l_1) \times (-l_2, l_2) \times (-l_3, l_3)$ such that ∇u takes only 4 different values for any t in the interval

$$1 \le t \le 1 + \frac{\gamma_3 - \gamma_2}{\gamma_2} \frac{l_2 - AR_0 l_3}{l_2} , \tag{3.37}$$

where

$$AR_0 = \frac{\gamma_2 + \gamma_3}{2\gamma_2} \left(\sqrt{1 + \frac{4\gamma_2\gamma_3}{(\gamma_2 + \gamma_3)^2}} - 1 \right) . \tag{3.38}$$

Proof. It is sufficient to construct $v(x_2, x_3)$ such that $v(\pm l_2, x_3) = \pm t\gamma_2 l_2 e_2 + \gamma_3 x_3 e_3$. Then one takes $u(x) = \gamma_1 x_1 e_1 + v(x_2, x_3)$. Figure 3.9 shows the regions where ∇v is constant, in the (x_2, x_3) plane. In the two regions denoted by A, which contain the portion of the boundary where the Dirichlet condition is imposed, we have $\nabla v = F_A = \mathrm{diag}(\gamma_2, \gamma_3)$. In the central region C, we have $\nabla v = F_C = \mathrm{diag}(\gamma_3, \gamma_2)$. In the regions denoted by B, $\nabla v = e^{i(\phi+\theta)}\mathrm{diag}(\gamma_2, \gamma_3)e^{-i\theta}$, where $e^{i\theta}$ denotes the matrix corresponding to a counterclockwise rotation by θ. The necessary conditions for the construction are that $F_A - F_B$ and $F_B - F_C$ are rank–one matrices, i.e.

$$\det(F_A - F_B) = \det(F_B - F_C) = 0\,, \tag{3.39}$$

and that the corresponding rank–one directions have a suitable orientation (i.e. one should also check that they are compatible with the global geometry displayed in Figure 3.9). Eq. (3.39) is equivalent to

$$\cos(\phi + 2\theta) = 0\,, \qquad \cos\phi = \frac{4\gamma_2\gamma_3}{(\gamma_3 + \gamma_2)^2}\,, \tag{3.40}$$

which has two pairs of opposite solutions, which we denote by $(\pm\phi, \pm\theta_1)$ and $(\pm\phi, \pm\theta_2)$. It remains to check that the corresponding rank–one direction have the relative orientation shown in the figure. Consider one of them, (ϕ, θ_1). Let ψ^{AB} and ψ^{BC} be the (uniquely defined) angles in $(0, \pi)$ such that $(F_A - F_B)(\cos\psi^{AB}, \sin\psi^{AB}) = (F_B - F_C)(\cos\psi^{BC}, \sin\psi^{BC}) = 0$ (ψ^{AB} and ψ^{BC} are the angles formed by the segments PR and PQ with the e_2 axis, respectively). If $\psi^{BC} \geq \psi^{AB}$ this solution is appropriate for B^+ (i.e. the part of B which is contained in the first and third quadrant). If instead $\psi^{BC} \leq \psi^{AB}$, this solution is appropriate for B^-. In both cases, $(-\phi, -\theta_1)$ gives a solution for the other half of B. The same reasoning applies to $(\pm\phi, \pm\theta_2)$, hence we have two solutions.

We now focus on one of them, with sign chosen so that $\psi^{BC} \geq \psi^{AB}$. The boundary condition is satisfied if and only if

$$t l_2 \gamma_2 = \gamma_3 P_2 + \gamma_2(l_2 - P_2) \tag{3.41}$$

where P_2 is the e_2 coordinate of the point P where the regions A and C touch. From the uniqueness of the elongation along e_2 (which is a consequence of the fact that ∇u is a gradient field),

$$\gamma_3 P_2 + \gamma_2(l_2 - P_2) = \gamma_3 Q_2 + (F_B)_{22}(R_2 - Q_2) + \gamma_2(l_2 - R_2)\,, \tag{3.42}$$

we then get, since $|(F_B)_{22}| \leq \gamma_3$ and $Q_2 \leq R_2$, that $P_2 \leq R_2$, i.e. $\psi^{AB} \in (0, \pi/2)$ (a more refined analysis indicates that $0 \leq \psi^{AB} \leq \pi/2 \leq \psi^{BC} \leq \pi$ for both solutions).

It remains to check that the entire construction can be fitted inside the domain. The topology displayed in the first panel of Figure 3.8 can be realized if and only if B^+ lies entirely in the part of Ω in the first quadrant, i.e. if and only if

$$0 \leq \min(Q_2, P_2, R_2) \leq \max(Q_2, P_2, R_2) \leq l_2 \,. \tag{3.43}$$

By a slight change in the connectivity of the domains, the first condition can actually be removed. Indeed, at least one of the two topologies of Figure 3.8 can be realized under the weaker condition

$$0 \leq P_2 \leq R_2 \leq l_2 \,. \tag{3.44}$$

Since $R_2 - P_2 = l_3 \cot \psi^{AB}$, this is possible only if the aspect ratio obeys

$$AR = \frac{l_2}{l_3} \geq AR_0 = \cot \psi^{AB} \,, \tag{3.45}$$

where a straightforward computation gives for AR_0 the expression (3.38). Then, from (3.41) we get a solution for

$$t - 1 = \frac{\gamma_3 - \gamma_2}{\gamma_2} \frac{P_2}{l_2} \tag{3.46}$$

i.e. for

$$1 \leq t \leq 1 + \frac{\gamma_3 - \gamma_2}{\gamma_2} \frac{AR - AR_0}{AR} \tag{3.47}$$

□

We finally compare the present construction with our numerical experiment, using the parameters from Section 3.3, i.e. $\gamma_2 = \gamma_3^{-1/2} = a^{1/6} = 2^{-1/6}$ and $l_2/l_3 = 1$ and 3. Then, one obtains $t_{\max}(AR = 3) \simeq 1.347$ and $t_{max}(AR = 1) \simeq 1.212$, which are both indistinguishable from the numerically obtained threshold within the numerical resolution (see Figure 3.4). The corresponding deformation for aspect ratio 3 is displayed in Figure 3.9.

3.5 Discussion and perspectives

In the previous sections we have presented a complete mathematical and numerical analysis of the predictions of the BTW model for stretching experiments on nematic elastomeric sheets. We now discuss the main results we have obtained, with particular attention to the possibility of comparing with experiment, with the aim not only to assess the general method but also to validate the specific assumptions we have made.

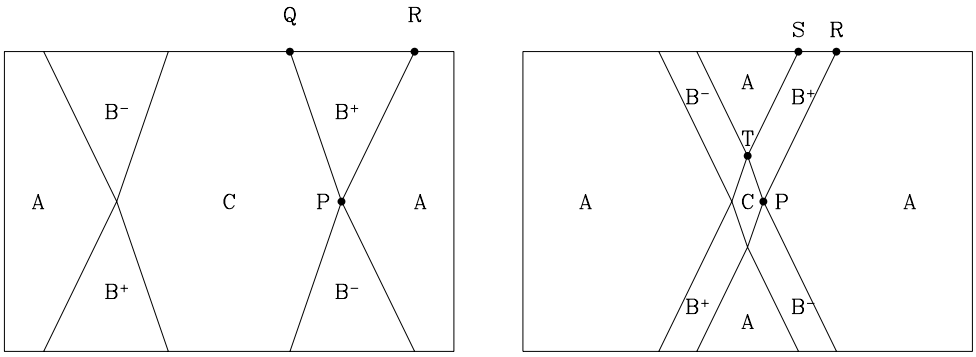

FIGURE 3.8: Construction of an energy minimizer u whose gradient takes finitely many values. The left panel shows the case where the first inequality in (3.44) is satisfied, the right panel a case where it is not satisfied (see Section 3.4.2 for details).

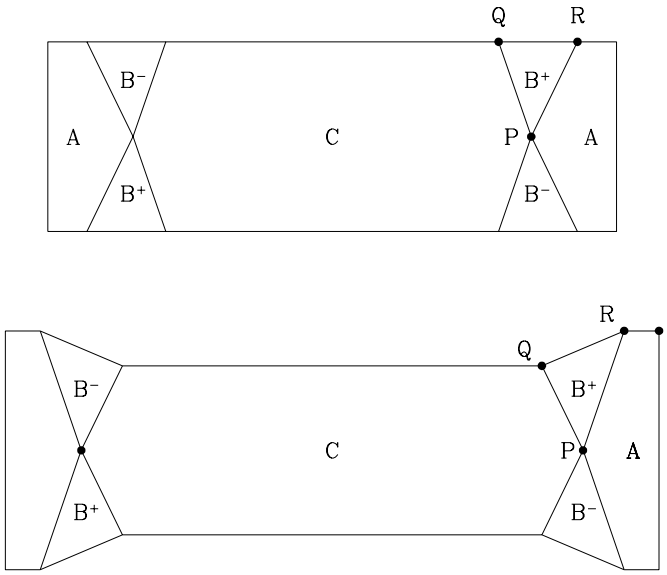

FIGURE 3.9: Construction of an energy minimizer u whose gradient takes finitely many values. The upper panel shows the reference configuration, the lower one the deformed configuration (see Section 3.4.2 for details). The figure has been drawn with $l_3/l_2 = 3$, $a = 1/2$.

We have shown that, up to a critical stretch, the material behaves as a liquid, in the sense that there is no reaction force to stretching, and the energy is constant. This has been shown both numerically, computing with finite elements based on the quasiconvexified energy, and analytically, by explicitly constructing functions on which the microscopic energy vanishes. The solutions constructed through the two approaches are different, and indeed there is a huge degeneracy: for stretches inside the liquid window there is a continuum of possible zero–energy solutions. This degeneracy has been lifted in the numerical procedure by adding an *ad hoc* regularizing term, which, however, has no physical justification. It is therefore natural to ask whether a more realistic selection mechanism could be obtained to single out the experimentally observed solution. From the point of view mentioned in the introduction, in this problem the robust quantities, which should not be largely affected by small perturbations, are the total energy and its derivative (the force of Figure 3.4). The deformation pattern and the microstructure are instead expected to be significantly affected by small perturbations.

We focus first on the robust quantity, the force, and observe that the general feature of a liquid–like response at small stretches, which is certainly the most interesting experimental result on these materials, is reproduced by the present theoretical approach. However, differences emerge in the details. Indeed, the small stiffness observed in experiments is missed by the BTW model, which gives exactly zero force at small strains.

Non–robust quantities, as for example the local microstructure, give a different picture. For example, at small strains the numerical solution predicts microstructure formation in all of the sample, whereas the analytical solution predicts no microstructure. One standard way to raise degeneracies is to include higher–order singular perturbations, either in the form of higher–order gradient terms or of surface–energy terms. However, this would immediately lead to the conclusion that the explicit construction of Section 3.4.2, with few interfaces, has lower energy than the solution with very fine structures of Section 3.3, which is in contrast with the experimental observation of fine–stripe patterns. A different, and probably more specific mechanism needs therefore to be considered.

A correction to the BTW energy which, in principle, can account for all the mentioned effects was proposed by Verwey, Warner, and Terentjev in 1996 [59, 61]. They suggested that in computing the average of Eq. (3.5) one should also average over fluctuations of a in the cross–linking configuration. By expansion of the product $\mathrm{Tr}\, U_n^{-2} F U_{n_0}^2 \tilde{F}^T$ and using the definition of U_n

one gets

$$\begin{aligned} \operatorname{Tr} U_n^{-2}\tilde{F}U_{n_0}^2\tilde{F}^T &= |\tilde{F}|^2 + (a-1)|\tilde{F}^T n|^2 + (a^{-1}-1)|\tilde{F}n_0|^2 \\ &\quad +(2-a-a^{-1})(n\tilde{F}n_0)^2 \end{aligned} \tag{3.48}$$

which then needs to be averaged over the distribution of a. The special symmetry present in W_{BTW} is only recovered if $\langle 1/a\rangle = 1/\langle a\rangle$. However, it is still possible to eliminate one of the terms in (3.48) by choosing a suitable reference configuration. More precisely, we write

$$\tilde{F} = Fb^{1/6}\left[\mathrm{Id} + (b^{-1/2}-1)n_0\otimes n_0\right] \tag{3.49}$$

substitute into (3.48), expand, and choose b so that the coefficient of $|nFn_0|^2$ vanishes, i.e.

$$b = \frac{\langle \frac{1}{a}\rangle - 1}{1-\langle a\rangle}\,. \tag{3.50}$$

Minimizing over n, and choosing $b^{1/3}k_BT/2$ as energy units, we get

$$W_{\mathrm{VWT}}(F) = \lambda_1^2(F) + \lambda_2^2(F) + \langle a\rangle\lambda_3^2(F) - \beta|Fn_0|^2 \tag{3.51}$$

where

$$\beta = \frac{\langle a\rangle\langle \frac{1}{a}\rangle - 1}{\langle \frac{1}{a}\rangle - 1} \tag{3.52}$$

is a nonnegative parameter which characterizes the strength of the anisotropy. This energy reduces to the BTW one if $\beta = 0$, i.e. if the distribution of a is a Dirac delta. The energy W_{VWT} is no longer invariant under rotations, and indeed states where the elongation direction is close to n_0 are favored. The consequences of the new term in (3.51) have been analyzed within a restricted geometry in [59, 61], to which we refer for a more detailed discussion. We only observe here that replacing W_{BTW} with W_{VWT} does not change at all the structure of the problem, since no additional gradients are included. However, the explicit computation of the quasiconvex envelope is a much harder problem for the non–isotropic W_{VWT} than it was for W_{BTW}. A full mathematical treatment of W_{BTW}, including computation of the quasiconvex envelope, is, in our opinion, one of the most interesting open questions in the mathematical analysis of nematic elastomers.

Acknowledgments

We thank R. V. Kohn for stimulating discussions, and R. Schäfer for the experimental results displayed in Figures 2.2 and 2.3. This work was partially supported by the EU TMR network *Phase Transitions in Crystalline Solids*, contract FMRX–CT98–0229, and by the NSF through grant DMS0104118. The third author was partially supported by the Max Planck Society.

References

[1] G. Alberti and S. Müller, *A new approach to variational problems with multiple scales*, Comm. Pure Appl. Math. **54** (2001), 761–825.

[2] L. Ambrosio, C. De Lellis, and C. Mantegazza, *Line energies for gradient vector fields in the plane*, Calc. Var. Partial Diff. Eqs. **9** (1999), 327–355.

[3] G. Anzellotti, S. Baldo, and A. Visintin, *Asymptotic behavior of the Landau–Lifshitz model of ferromagnetism*, Appl. Math. Optim. **23** (1991), 171–192.

[4] J. Ball and R. D. James, *Fine phase mixtures as minimizers of the energy*, Arch. Rat. Mech. Anal. **100** (1987), 13–52.

[5] H. Ben Belgacem, S. Conti, A. DeSimone, and S. Müller, *Energy scaling of compressed elastic films*, Preprint MPI–MIS 83 (2001).

[6] ———, *Rigorous bounds for the Föppl–von Kármán theory of isotropically compressed plates*, J. Nonlinear Sci. **10** (2000), 661–683.

[7] H. A. M. van den Berg, *Self–consistent domain theory in soft–ferromagnetic media. ii. basic domain structures in thin film objects*, J. Appl. Phys. **60** (1986), 1104–1113.

[8] G. Bertotti, *Hysteresis in magnetism*, Academic Press, San Diego, 1998.

[9] P. Bladon, E. M. Terentjev, and M. Warner, *Transitions and instabilities in liquid–crystal elastomers*, Phys. Rev. E **47** (1993), R3838–R3840.

[10] A. Braides and A. Defranceschi, *Homogeneization of multiple integrals*, Claredon Press, Oxford, 1998.

[11] W. F. Brown, *Micromagnetics*, Wiley, 1963.

[12] P. Bryant and H. Suhl, *Thin–film magnetic patterns in an external field*, Appl. Phys. Lett. **54** (1989), 2224.

[13] M. Chipot and D. Kinderlehrer, *Equilibrium configurations of crystals*, Arch. Rat. Mech. Anal. **103** (1988), 237–277.

[14] S. Conti, G. Dolzmann, and A. DeSimone, *Soft elastic response of stretched sheets of nematic elastomers: a numerical study*, J. Mech. Phys. Solids (in press).

[15] B. Dacorogna, *A relaxation theorem and its application to the equilibrium of gases*, Arch. Rat. Mech. Anal. **77** (1981), 359–386.

[16] _____, *Direct methods in the calculus of variations*, Springer, Berlin, 1989.

[17] B. Dacorogna and C. Tanteri, *Implicit partial differential equations and the constraints of non linear elasticity*, Comm. in PDEs (2001), in press.

[18] G. Dal Maso, *An introduction to* Γ*–convergence*, Birkhäuser, Boston, 1993.

[19] E. De Giorgi, *Sulla convergenza di alcune successioni di integrali del tipo dell'area*, Rend. Mat. **8** (1975), 277–294.

[20] E. De Giorgi and T. Franzoni, *Su un tipo di convergenza variazionale*, Atti Accad. Naz. Lincei Rend. Cl. Sci. Mat. **58** (1975), 842–850.

[21] A. DeSimone and G. Dolzmann, *Macroscopic response of nematic elastomers via relaxation of a class of* $SO(3)$*–invariant energies*, Arch. Rat. mech. Anal. (in press).

[22] A. DeSimone and R. D. James, *A constrained theory of magnetoelasticity*, J. Mech. Phys. Solids (in press).

[23] A. DeSimone, R. V. Kohn, S. Müller, and F. Otto, *A compactness result in the gradient theory of phase transitions*, Proc. Roy. Soc. Edin. A **131** (2001), 833–844.

[24] _____, *Magnetic microstructures – a paradigm of multiscale problems*, ICIAM 99 (J. M. Ball and J. C. R. Hunt, eds.), Oxford Univ. Press, 2000, pp. 175–190.

[25] _____, *A reduced theory for thin–film micromagnetics*, Preprint MPI–MIS 82 (2001).

[26] ———, *Repulsive interaction of Néel wall tails*, in preparation.

[27] A. DeSimone, R.V. Kohn, S. Müller, F. Otto, and R. Schäfer, *Two–dimensional modeling of soft ferromagnetic films*, Proc. Roy. Soc. Lond. (in press).

[28] L.C. Evans, *Partial differential equations*, American Mathematical Society, Providence, 1998.

[29] H. Finkelmann, I. Kundler, E. M. Terentjev, and M. Warner, *Critical stripe–domain instability of nematic elastomers*, J. Phys. II France **7** (1997), 1059–1069.

[30] G. Friesecke, R. James, and S. Müller, *Rigorous derivation of nonlinear plate theory and geometric rigidity*, C. R. Acad. Sci. Paris Série I (to appear).

[31] G. Friesecke and F. Theil, *Validity and failure of the Cauchy–Born hypothesis in a 2D mass–spring lattice*, preprint (2001).

[32] C. J. García–Cervera and W. E, *Effective dynamics for ferromagnetic thin films*, J. Appl. Phys. **90** (2001), 370–374.

[33] P. Gérard, *Microlocal defect measures*, Comm. PDE **16** (1991), 1761–1794.

[34] G. Gioia and M. Ortiz, *Delamination of compressed thin films*, Adv. Appl. Mech. **33** (1997), 119–192.

[35] L. Golubović and T. C. Lubensky, *Nonlinear elasticity of amorphous solids*, Phys. Rev. Lett. **63** (1989), 1082–1085.

[36] A. Hubert and R. Schäfer, *Magnetic domains*, Springer, Berlin, 1998.

[37] P. E. Jabin, F. Otto, and B. Perthame, *Line–energy Ginzburg–Landau models: zero–energy states*, subm. to Ann. Sc. Normale Pisa (2001).

[38] P. E. Jabin and B. Perthame, *Compactness in Ginzburg–Landau energy by kinetic averaging*, Comm. Pure Appl. Math. **54** (2001), 1096–1109.

[39] V. V. Jikov, S. M. Kozlov, and O. A. Oleinik, *Homogeneization of differential operators and integral functionals*, Springer, Berlin, 1994.

[40] W. Jin and R. V. Kohn, *Singular perturbation and the energy of folds*, J. Nonlinear Sci. **10** (2000), 355–390.

[41] W. Jin and P. Sternberg, *Energy estimates of the von Kármán model of thin–film blistering*, J. Math. Phys. **42** (2001), 192–199.

[42] J. Kundler and H. Finkelmann, *Strain–induced director reorientation in nematic liquid single crystal elastomers*, Macromol. Chem. Rapid Comm. **16** (1995), 679–686.

[43] L. D. Landau and E. M. Lifshitz, *On the theory of the dispersion of magnetic permeability in ferromagnetic bodies*, Phys Z. Sowjetunion **8** (1935), 153–169.

[44] C. Le Bris and X. Blanc amd P.–L. Lions, *Convergence de modèles moléculaires vers des modèles de mécanique des milieux continus*, C. R. Acad. Sci. Paris Série I **332** (2001), 949–956.

[45] C. Melcher, *The logarithmic tail of Néel walls in thin films*, Preprint MPI–MIS 61 (2001).

[46] C. B. Morrey, *Multiple integrals in the calculus of variations*, Springer, Berlin, 1966.

[47] S. Müller, *Variational models for microstructure and phase transitions*, in Calculus of Variations and Geometric Evolution Problems, Le ctures given at the 2nd Session of the Centro Internazionale Matematico Estivo, Cetaro 1996 (F. Bethuel, G. Huisken, S. Müller, K. Steffen, S. Hildebrandt, and M. Struwe, eds.), Springer, Berlin, 1999.

[48] S. Müller and V. Šverák, *Convex integration with constraints and applications to phase transitions and partial differential equations*, J. Eur. Math. Soc. (JEMS) **1** (1999), 393–442.

[49] F. Murat and L. Tartar, *Calcul des variations et homogénéisation*, Les Méthodes de l'Homogénéisation: Théorie et Applications en Physique (D. Bergman et al., ed.), Collect. Dir. Etudes Rech. Electricité de France, vol. 57, Eyrolles, Paris, 1985, pp. 319–369, (translated in [50]).

[50] ———, *Calculus of variations and homogenization*, Topics in the Mathematical Modelling of Composite Materials (A. Cherkaev and R. Kohn, eds.), Progress in Nonlinear Differential Equations and Their Applications, Birkhäuser, Boston, 1997, pp. 139–173, (see also the other contributions in this volume).

[51] O. Pantz, *Une justification partielle du modèle de plaque en flexion par* Γ*–convergence*, C. R. Acad. Sci. Paris Série I **332** (2001), 587–592.

[52] T. Rivière and S. Serfaty, *Limiting domain wall energy for a problem related to micromagnetics*, Comm. Pure Appl. Math. **54** (2001), 294–338.

[53] J. A. Sethian, *Level set methods*, Cambridge University Press, 1996.

[54] M. Šilhavý, *Relaxation in a class of $SO(n)$-invariant energies related to nematic elastomers*, preprint (2001).

[55] L. Tartar, *Compensated compactness and partial differential equations*, Nonlinear analysis and mechanics: Heriot–Watt Symposium (R. Knops, ed.), vol. IV, Pitman, 1979, pp. 136–212.

[56] ———, *H–measures, a new approach for studying homogenization, oscillations and concentration effects in partial differential equations*, Proc. Roy. Soc. Edin. A **115** (1990), 193–230.

[57] ———, *Beyond Young measures*, Meccanica **30** (1995), 505–526.

[58] R. Tickle, R.D. James, T. Shield, M. Wuttig, and V.V. Kokorin, *Ferromagnetic shape memory in the NiMnGa system*, IEEE Trans. Magn. **35** (1999), 4301–4310.

[59] G. C. Verwey, M. Warner, and E. M. Terentjev, *Elastic instability and stripe domain in liquid crystalline elastomers*, J. Phys. II France **6** (1996), 1273–1290.

[60] M. Warner, *New elastic behaviour arising from the unusual constitutive relation of nematic solids*, J. Mech. Phys. Sol. **47** (1999), 1355–1377.

[61] M. Warner and E. M. Terentjev, *Nematic elastomers – a new state of matter?*, Prog. Polym. Sci. **21** (1996), 853–891.

[62] J. Weilepp and H. R. Brand, *Director reorientation in nematic–liquid–single–crystal elastomers by external mechanical stress*, Europhys. Lett. **34** (1996), 495–500.

[63] L. C. Young, *Lectures on the calculus of variations and optimal control theory*, Saunders, 1969, reprinted by Chelsea, 1980.

[64] E. R. Zubarev, S. A. Kuptsov, T. I. Yuranova, R. V. Talroze, and H. Finkelmann, *Monodomain liquid crystalline networks: reorientation mechanism from uniform to stripe domains*, Liquid crystals **26** (1999), 1531–1540.